

The Solar Twin Planet Search

IV. The Sun as a typical rotator and evidence for a new rotational braking law for Sun-like stars^{*}

Leonardo A. dos Santos^{1,2}, Jorge Meléndez¹, José-Dias do Nascimento Jr.^{3,4}, Megan Bedell², Iván Ramírez⁵, Jacob L. Bean², Martin Asplund⁶, Lorenzo Spina¹, Stefan Dreizler⁷, Alan Alves-Brito⁸, and Luca Casagrande⁶

¹ Universidade de São Paulo, Departamento de Astronomia do IAG/USP, Rua do Matão 1226, Cidade Universitária, 05508-900 São Paulo, SP, Brazil
e-mail: leonardoags@usp.br

² University of Chicago, Department of Astronomy and Astrophysics, USA

³ Universidade Federal do Rio Grande do Norte, 59072-970 Natal, RN, Brazil

⁴ Harvard-Smithsonian Center for Astrophysics, Cambridge, MA 02138, USA

⁵ University of Texas, McDonald Observatory and Department of Astronomy at Austin, USA

⁶ The Australian National University, Research School of Astronomy and Astrophysics, Cotter Road, Weston, ACT 2611, Australia

⁷ University of Göttingen, Institut für Astrophysik, Germany

⁸ Universidade Federal do Rio Grande do Sul, Instituto de Física, Av. Bento Gonçalves 9500, Porto Alegre, RS, Brazil

Received 19 March 2016; accepted 20 June 2016

ABSTRACT

Context. It is still unclear how common the Sun is when compared to other similar stars in regards to some of its physical properties, such as rotation. Considering that gyrochronology relations are widely used today to estimate ages of stars in the main sequence, and that the Sun is used to calibrate it, it is crucial to assess if these procedures are acceptable.

Aims. We analyze the rotational velocities – limited by the unknown rotation axis inclination angle – of an unprecedented large sample of solar twins in order to study the rotational evolution of Sun-like stars, and assess if the Sun is a typical rotator.

Methods. We use high-resolution ($R = 115000$) spectra obtained with the HARPS spectrograph and ESO's 3.6 m telescope at La Silla Observatory. The projected rotational velocities for 82 solar twins are estimated by line profile fitting with synthetic spectra. Macroturbulence velocities are inferred from a prescription that accurately reflects their dependence with effective temperature and luminosity of the stars.

Results. Our sample of solar twins include some spectroscopic binaries with enhanced rotational velocities, and we do not find any non-spectroscopic binaries with unusually high rotation velocities. We verified that the Sun does not have a peculiar rotation, but the solar twins exhibit rotational velocities that depart from the Skumanich relation.

Conclusions. The Sun is a regular rotator when compared to solar twins with a similar age. Additionally, we obtain a rotational braking law that better describes the stars in our sample ($v \propto t^{-0.6}$) in contrast to previous, often-used scalings.

Key words. Sun: rotation – stars: solar-type – stars: rotation – stars: fundamental parameters

1. Introduction

The Sun is the best known star to astronomers, and is commonly used as a template in the study of other similar objects. Yet, there are still some of its aspects that are not well understood and that are crucial for a better understanding of how stars, and consequently how planetary systems and life evolve: how do the more complex physical parameters of a Sun-like star, such as rotation and magnetic activity, change with time? Is the Sun unique or typical (i.e., an average Sun-like star)? If the Sun is common, it would mean that life does not require a special star for it to

flourish, eliminating the need to evoke an anthropic reasoning to explain it.

In an effort to assess how typical the Sun is, Robles et al. (2008) compared 11 of its physical parameters with nearby stars, and concluded that the Sun is, in general, typical. Although they found it to be a slow-rotator against 276 F8 – K2 (within $\pm 0.1 M_{\odot}$) nearby stars, this result may be rendered inconclusive owing to unaccounted noise caused by different masses and ages in their sample. Other studies have suggested that the Sun rotates either unusually slow (Smith 1979; Leão et al. 2015) or regularly for its age (Soderblom 1983, 1985; Gray 1984; Gustafsson 1998; Barnes 2003), but none of them comprised stars that are very similar to the Sun, therefore preventing a reliable comparison. In fact, with *Kepler* and *CoRoT*, it is now possible to obtain precise measurements of rotation periods, masses and ages of stars in a very homogeneous way (e.g., Ceillier et al. 2015; do Nascimento et al. 2012; Chaplin et al. 2014), but they generally lack high precision stellar parameters, which are accessible through

^{*} Based on observations collected at the European Organisation for Astronomical Research in the Southern Hemisphere under ESO programs 188.C-0265, 183.D-0729, 292.C-5004, 077.C-0364, 072.C-0488, 092.C-0721, 093.C-0409, 183.C-0972, 192.C-0852, 091.C-0936, 089.C-0732, 091.C-0034, 076.C-0155, 185.D-0056, 074.C-0364, 075.C-0332, 089.C-0415, 60.A-9036, 075.C-0202, 192.C-0224, 090.C-0421 and 088.C-0323.

spectroscopy. The challenging nature of these observations limited ground-based efforts to smaller, but key stellar samples (e.g., Pizzolato et al. 2003; Strassmeier et al. 2012).

The rotational evolution of a star plays a crucial role in stellar interior physics and habitability. Previous studies proposed that rotation can produce extra mixing that is responsible for depleting the light elements Li and Be in their atmospheres (Pinsonneault et al. 1989; Charbonnel et al. 1994; Tucci Maia et al. 2015), which could explain the disconnection between meteoritic and solar abundances of Li (Baumann et al. 2010). Moreover, rotation is highly correlated with magnetic activity (e.g., Noyes et al. 1984; Soderblom et al. 1993; Baliunas et al. 1995; Mamajek & Hillenbrand 2008), and this trend is key to understand how planetary systems and life evolve in face of varying magnetic activity and energy outputs by solar-like stars during the main sequence (Guinan & Engle 2009; Ribas et al. 2005; do Nascimento et al. 2016).

A theoretical treatment of rotational evolution from first principles is missing, so we often rely on empirical studies to infer about it. One of the pioneer efforts in this endeavor produced the well known Skumanich relation $v \propto t^{-1/2}$, where v is the rotational velocity and t is the stellar age (Skumanich 1972), which describes the rotational evolution of solar-type stars in the main sequence, and can be derived from the loss of angular momentum due to magnetized stellar winds (e.g., Kawaler 1988; Charbonneau 1992; Barnes 2003; Gallet & Bouvier 2013). This relation sparked the development of gyrochronology, which consists in estimating stellar ages based on their rotation, and it was shown to provide a stellar clock as good as chromospheric ages (Barnes 2007). However, in Skumanich-like relations, the Sun generally falls on the curve (or plane, if we consider dependence on mass) defined by the rotational braking law by design. Thus it is of utmost importance to assess how common the Sun is in order to correctly calibrate it.

Subsequent studies have proposed modifications to this paradigm of rotation and chromospheric activity evolution (e.g., Soderblom et al. 1991; Pace & Pasquini 2004), exploring rotational braking laws of the form $v \propto t^{-b}$. The formalism by Kawaler (1988) shows that this index b can be related to the geometry of the stellar magnetic field, and that Skumanich's index ($b = 1/2$) corresponds to a geometry that is slightly more complex than a simple radial field. It also dictates the dependence of the angular momentum on the rotation rate, and in practice, it determines how early the effects of braking are felt by a model. Such prescriptions for rotational evolution have a general agreement for young ages up to the solar age (see Sood et al. 2016; Amard et al. 2016, and references therein), but the evolution for older ages still poses an open question. In particular, van Saders et al. (2016) suggested that stars undergo a weakened magnetic braking after they reach a critical value of the Rossby number, thus explaining the stagnation trend observed on the rotational periods of older Kepler stars.

In order to assess how typical the Sun is in its rotation, our study aims to verify if it follows the rotational evolution of stars that are very similar to it, an objective that is achieved by precisely measuring their rotational velocities and ages. We take advantage of an unprecedented large sample of solar twins (Ramírez et al. 2014) using high signal-to-noise ($S/N > 500$) and high resolution ($R > 10^5$) spectra, which provides us with precise stellar parameters and is essential for the analysis that we perform (see Fig. 1 for an illustration of the subtle effects of rotation in stellar spectra of Sun-like stars).

2. Working sample

Our sample consists of bright solar twins in the Southern Hemisphere, which were mostly observed in our HARPS Large Program (ID: 188.C-0265) that aimed to search for planetary systems around stars very similar to the Sun (Ramírez et al. 2014; Bedell et al. 2015; Tucci Maia et al. 2016, Papers I, II and III, respectively, of the series The Solar Twin Planet Search). These stars are loosely defined as those that have T_{eff} , $\log g$ and $[\text{Fe}/\text{H}]$ inside the intervals ± 100 K, ± 0.1 [cgs] and 0.1 dex, respectively, around the solar values. It has been shown that these limits guarantee ~ 0.01 dex precision in the relative abundances derived using standard model atmosphere methods and that the systematic uncertainties of that analysis are negligible within those ranges (Bedell et al. 2014; Biazzo et al. 2015; Saffe et al. 2015; Yana Galarza et al. 2016). In total, we obtained high precision spectra for 73 stars and used data from 9 more targets observed in other programs, all of them overlapping the sample of 88 stars from Paper I. We used the spectrum of the Sun (reflected light from the Vesta asteroid) from the ESO program 088.C-0323, which was obtained with the same instrument and configuration as the solar twins.

The ages of the solar twin sample span between 0 – 10 Gyr and are presented in the online material (Table 3). They were obtained by Tucci Maia et al. (2016) using Yonsei-Yale isochrones (Yi et al. 2001) and probability distribution functions as described in Ramírez et al. (2013, 2014). Uncertainties are assumed to be symmetric. These ages are in excellent agreement with the ones obtained in Paper I, with a mean difference of -0.1 ± 0.2 Gyr (see footnote 5 in Paper III). We adopted 4.56 Gyr for the solar age (Bahcall et al. 1995). The other stellar parameters (T_{eff} , $\log g$, $[\text{Fe}/\text{H}]$ and microturbulence velocities v_t) were obtained by Ramírez et al. (2014). The stellar parameters of HIP 68468 and HIP 108158 were updated by Tucci Maia et al. (2016).

Our targets were observed at the HARPS spectrograph¹ (Mayor et al. 2003) which is fed by ESO's 3.6 m telescope at La Silla Observatory. When available publicly, we also included all observations from other programs in our analysis in order to increase the signal to noise ratio (S/N) of our spectra. However, we did not use observations for 18 Sco (HIP 79672) from May 2009² and we did not include observations post-HARPS upgrade (June 2015) when combining the spectra³.

The wavelength coverage for the observations ranged from 3780 to 6910 Å, with a spectral resolving power of $R = \lambda/\Delta\lambda = 115000$. Data reduction was performed automatically with the HARPS Data Reduction Software (DRS). Each spectrum was divided in two halves, corresponding to the mosaic of two detectors (one optimized for the blue and other for the red wavelengths). In this study we only worked with the red part (from 5330 to 6910 Å) due to its higher S/N and the presence of cleaner lines. The correction for radial velocities was performed with the task `dopcor` from IRAF⁴, using the values obtained

¹ The initial plan was to use the observations from the MIKE spectrograph, as described by the Paper I. However, we decided to use the HARPS spectra due to its higher spectral resolving power.

² These observations have instrumental artifacts.

³ The spectra had a different shape in the red side, and since there were few observations, we chose not to use them to eliminate eventual problems with combination and normalization.

⁴ IRAF is distributed by the National Optical Astronomy Observatories, which are operated by the Association of Universities for Research in Astronomy, Inc., under cooperative agreement with the National Science Foundation.

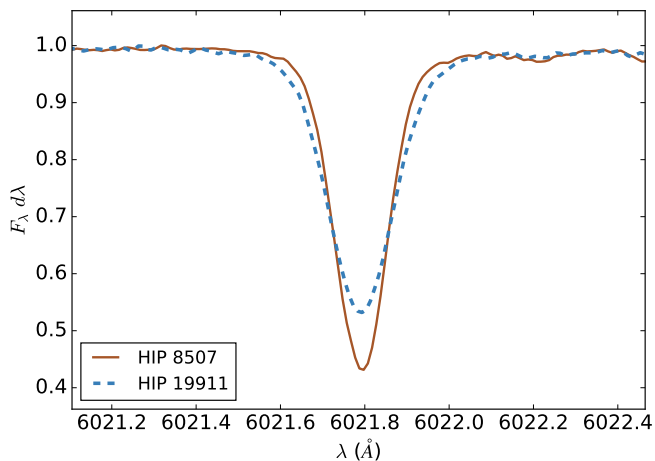


Fig. 1. Comparison of the spectral line broadening between two solar twins with different projected rotational velocities. The wider line corresponds to HIP 19911, with $v \sin i \approx 4.1 \text{ km s}^{-1}$, and the narrower one comes from HIP 8507, with $v \sin i \approx 0.8 \text{ km s}^{-1}$.

from the pipeline’s cross-correlation function (CCF) data. The different observations were combined with IRAF’s `scombine`. The resulting average (of the sample) signal to noise ratio was 500 around 6070 Å. The red regions of the spectra were normalized with ~ 30 th order polynomial fits to the upper envelopes of the entire red range, using the task `continuum` on IRAF. We made sure that the continuum of the stars were consistent with the Sun’s. Additionally, we verified that errors in the continuum determination introduce uncertainties in $v \sin i$ lower than 0.1 km s^{-1} .

3. Methods

We analyze five spectral lines, four due to Fe I and one to Ni I (see Table 1; equivalent widths were measured using the task `splot` in IRAF), that were selected for having low level of contamination by blending lines. The rotational velocity of a star can be measured by estimating the spectral line broadening that is due to rotation. The rotation axes of the stars are randomly oriented, thus the spectroscopic measurements of rotational velocity are a function of the inclination angle ($v \sin i$).

Table 1. Line list used in the projected stellar rotation measurements.

Wavelength (Å)	Z	Exc. pot. (eV)	$\log(gf)$	v_{macro}^{\odot} (km s^{-1})	EW $^{\odot}$ (Å)
6027.050	26	4.076	-1.09	3.0	0.064
6151.618	26	2.176	-3.30	3.2	0.051
6165.360	26	4.143	-1.46	3.1	0.045
6705.102	26	4.607	-0.98	3.6	0.047
6767.772	28	1.826	-2.17	2.9	0.079

Notes. EW are the equivalent widths and v_{macro} are the macroturbulence velocities measured as in Sect. 3.1.

We estimate $v \sin i$ for our sample of solar twins using the 2014 version of MOOG Synth (Snedden 1973), adopting stellar atmosphere models by Castelli & Kurucz (2004), with interpolations between models performed automatically by the

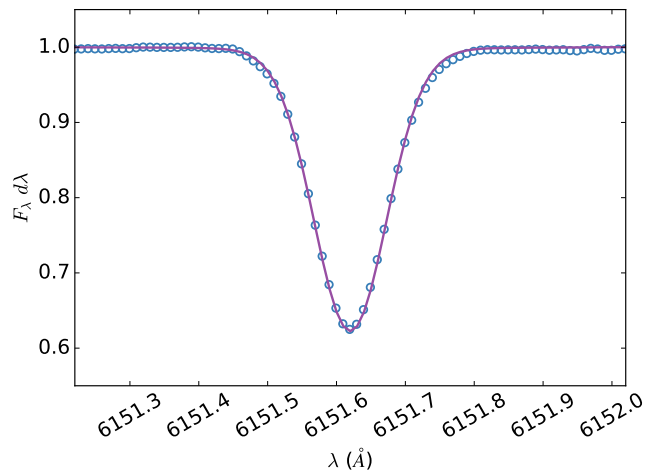


Fig. 2. Example of line profile fitting for the Fe I feature at 6151.62 Å in the spectrum of the Sun. The continuous curve is the synthetic spectrum, and the open circles are the observed data.

Python package `qoyllur-quipu`⁵ (see Ramírez et al. 2014). The instrumental broadening is taken into account by the spectral synthesis. We used the stellar parameters from Tucci Maia et al. (2016) and macroturbulence velocities from Ramírez et al. (2014). Macroturbulence velocities (v_{macro}) were calculated by scaling the solar values, line by line (see Sect. 3.1). Estimation of the rotational velocities was performed with our own algorithm⁶ that makes automatic measurements for all spectral lines for each star. We applied fine tuning corrections by eye for the non-satisfactory automatic line profile fittings, and quote $v \sin i$ as the mean of the values measured for the five lines. See Sects. 3.1 and 3.2 for a detailed description on rotational velocities estimation as well as their uncertainties. Fig. 2 shows an example of spectral line fitting for one feature in the Sun.

3.1. Macroturbulence velocities

We tested the possibility of measuring v_{macro} (radial-tangential profile) simultaneously with $v \sin i$, but even when using the extremely high-resolution spectra of HARPS, it is difficult to disentangle these two spectral line broadening processes, which is probably due to the low values of these velocities. Macroturbulence has a stronger effect on the wings of the spectral lines, but our selection of clean lines still has some contamination that requires this high-precision work to be done by eye. Some stars show more contamination than others, complicating the disentanglement. Fortunately, the variation of macroturbulence with effective temperature and luminosity is smooth (Gray 2005), so that precise values of v_{macro} could be obtained by a calibration. Thus we adopted a relation that fixes macroturbulence velocities in order to measure $v \sin i$ with high precision using an automatic code, which provides the additional benefits of reproducibility and lower stability.

The macroturbulence velocity is known to vary for different spectral lines (Gray 2005), so for our high-precision analysis, we do not adopt a single value for each star. Instead, we measure the v_{macro} for the Sun in each of the spectral lines from Table 1,

⁵ Available at <https://github.com/astroChasqui/q2>

⁶ Available at <https://github.com/RogueAstro/POWeRS>

and use these values to scale the v_{macro} for all stars in our sample using the following equation⁷:

$$v_{\text{macro},\lambda}^* = v_{\text{macro},\lambda}^{\odot} - 0.00707 T_{\text{eff}} + 9.2422 \times 10^{-7} T_{\text{eff}}^2 + 10.0 + k_1 (\log g - 4.44) + k_2 \quad (1)$$

$$\equiv f(T_{\text{eff}}) + k_1 (\log g - 4.44) + k_2$$

where $v_{\text{macro},\lambda}^{\odot}$ is the macroturbulence velocity of the Sun for a given spectral line, T_{eff} and $\log g$ are, respectively, the effective temperature and gravity of a given star, k_1 is a proportionality factor for $\log g$ and k_2 is a small correction constant.

This formula is partly based on the relation derived by Meléndez et al. (2012) (Eq. E.1 in their paper) from the trend of macroturbulence with effective temperature in solar-type stars described by Gray (2005). The $\log g$ -dependent term (a proxy for luminosity) comes from the empirical relation derived by Doyle et al. (2014) (Eq. 8 in their paper), and is based on spectroscopic measurements of v_{macro} of *Kepler* stars, which were disentangled from $v \sin i$ using asteroseismic estimates of the projected rotational velocities. Doyle et al. obtained a value for the proportionality factor k_1 of -2.0. However their uncertainties on v_{macro} were of the order of 1.0 km s^{-1} . Thus, we decided to derive our own values of k_1 and k_2 by simultaneously measuring v_{macro} and $v \sin i$ of a sub-sample of solar twins.

This sub-sample was chosen to contain only single stars or visual binaries mostly in the extremes of $\log g$ (4.25 – 4.52) in our entire sample. We assume these values to have a linear relationship with v_{macro} inside this short interval of $\log g$. We used as a first guess the values of $v \sin i$ and v_{macro} from a previous, cruder estimation we made, and performed line profile fits by eye using MOOG Synth. The velocities in Table 2 are the median of the values measured for each line and their standard error. Note that these $v \sin i$ are not consistently measured in the same way that the final results are. The rotational velocity broadening was calculated by our own code (see Sect. 3.2 for details). By performing a linear fit in the $v_{\text{macro}} - f(T_{\text{eff}})$ vs. $\log g - 4.44$ relation (f comprises all the T_{eff} -dependent terms, the macroturbulence velocity of the Sun and the known constant on Eq. 2), we obtain that $k_1 = -1.81 \pm 0.26$ and $k_2 = -0.05 \pm 0.03$ (see Fig. 3). For the stars farthest from the Sun in $\log g$ from our sample, these values of k_1 and k_2 would amount to differences of up to $\pm 0.4 \text{ km s}^{-1}$ in their macroturbulence velocities, therefore it is essential to consider the luminosity effect on v_{macro} for accurate $v \sin i$ determinations.

To obtain the macroturbulence velocities for the Sun to use in Eq. 2, we forced the rotational velocity of the Sun to 1.9 km s^{-1} (Howard & Harvey 1970), and then estimated values of $v_{\text{macro},\lambda}^{\odot}$ by fitting each line profile using MOOG Synth, and the results are shown in Table 1. We estimate the error in determining $v_{\text{macro},\lambda}^{\odot}$ to be $\pm 0.1 \text{ km s}^{-1}$. Since Eq. 2 is an additive scaling, the error for v_{macro} of all stars is the same as in the Sun⁸.

⁷ In the future, it should be possible to calibrate macroturbulence velocities using 3D hydrodynamical stellar atmosphere models (e.g., Magic et al. 2013) by using predicted 3D line profiles (without rotational broadening) as observations and determine which value of v_{macro} is needed to reproduce them with 1D model atmospheres.

⁸ The uncertainties in stellar parameters have contributions that are negligible compared to the ones introduced by the error in v_{macro} .

Table 2. Simultaneous measurements of rotational and macroturbulence velocities of stars in the extremes of $\log g$ from our sample of solar twins.

Star	$v \sin i$ (km s^{-1})	v_{macro} (km s^{-1})	T_{eff}	$\log g$
HIP 115577	0.95 ± 0.05	3.35 ± 0.09	5699	4.25
HIP 65708	1.20 ± 0.09	3.55 ± 0.08	5755	4.25
HIP 74432	1.40 ± 0.03	3.35 ± 0.08	5684	4.25
HIP 118115	1.40 ± 0.10	3.43 ± 0.09	5808	4.28
HIP 68468	1.75 ± 0.07	3.70 ± 0.08	5857	4.32
HIP 41317	1.55 ± 0.03	3.10 ± 0.06	5700	4.38
Sun	1.75 ± 0.07	3.30 ± 0.06	5777	4.44
HIP 105184	2.50 ± 0.03	3.21 ± 0.08	5833	4.50
HIP 10175	1.55 ± 0.06	3.05 ± 0.08	5738	4.51
HIP 114615	2.20 ± 0.03	3.25 ± 0.08	5816	4.52
HIP 3203	3.90 ± 0.03	3.40 ± 0.10	5850	4.52

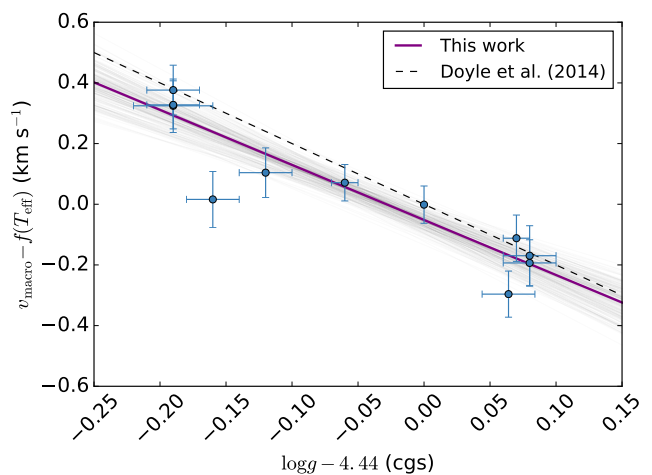


Fig. 3. Linear relation between v_{macro} and $\log g$ (a proxy for luminosity) for the stars on Table 2. See the definition of $f(T_{\text{eff}})$ in Sect. 3.1. The orange continuous line represents our determination of a proportionality coefficient of -1.81 and a vertical shift of -0.05 km s^{-1} . The black dashed line is the coefficient found by Doyle et al. (2014). The light grey region is a composition of 200 curves with parameters drawn from a multivariate gaussian distribution. The Sun is located at the origin.

3.2. Rotational velocities

Our code takes as input the list of stars and their parameters (effective temperature, surface gravity, metallicity and macroturbulence velocities obtained on Paper I), their spectra and the spectral line list in MOOG-readable format. For each line in a given star, the code automatically corrects the spectral line shift and the continuum. The first is done by fitting a second order polynomial to the kernel of a line and estimating what distance the observed line center is from the laboratory value. Usually, the spectral line shift corrections were of the order of 10^{-2} \AA , corresponding to 0.5 km s^{-1} in the wavelength range we worked on. This is a reasonable shift that likely arises from a combination of granulation and gravitational redshift effects, which are of similar magnitude. The continuum correction for each line is defined as the value of a multiplicative factor that sets the highest flux inside a radius of 2.5 \AA around the line center to 1.0. The multiplicative factor usually has a value inside the range 1.000 ± 0.002 .

The code starts with a range of $v \sin i$ and abundances and optimizes these two parameters through a series of iterations that measure the least squares difference between the observed line and the synthetic line (generated with MOOG synth). Convergence is achieved when the difference between the best solution and the previous one, for both $v \sin i$ and abundance, is less than 1%. Additionally, the code also forces at least 10 iterations in order to avoid falling into local minima.

One of the main limitations of MOOG Synth for our analysis is that it has a "quantized" behavior for $v \sin i$: the changes in the synthetic spectra occur most strongly in steps of 0.5 km s^{-1} . This behavior is not observed in varying the macroturbulence velocities. Therefore, we had to incorporate a rotational broadening routine in our code that was separated from MOOG. We used the Eq. 18.14 from Gray (2005), in velocity space, to compute the rotational profile⁹:

$$G(v) = \frac{2(1 - \epsilon) \left[1 - (v/v_L)^2 \right]^{1/2} + \frac{1}{2} \pi \epsilon \left[1 - (v/v_L)^2 \right]}{\pi v_L (1 - \epsilon/3)}, \quad (2)$$

where v_L is the projected rotational velocity and ϵ is the limb darkening coefficient (for which we adopt the value 0.6). The rotational profile $G(v)$ is then convolved with MOOG's synthetic profiles (which were generated with $v \sin i = 0$).

The total uncertainties in rotational velocities are obtained from the quadratic sum of the standard error of the five measurements and an uncertainty of 0.1 km s^{-1} introduced by the error in macroturbulence velocities. Systematic errors in the calculation of $v_{\text{macro},l}$ for the stars do not significantly contribute to the $v \sin i$ uncertainties.

Some of the stars in the sample show very low rotational velocities, most probably due to the effect of projection (see left panel of Fig. 5). The achieved precision is validated by comparison with the values of the full-width at half maximum (FWHM) measured by the cross-correlation function (CCF) from the data reduction pipeline, with the effects of macroturbulence subtracted (see Fig. 4). The spectroscopic binary star HIP 103983 has an unusually high $v \sin i$ when compared to the CCF FWHM, and a verification of its spectral line profiles reveals the presence of distortions that are the most probably caused by mis-measurement of rotational velocity (contamination of the combined spectrum by a companion – observations range from October 2011 to August 2012). We obtained a curve fit for the $v \sin i$ vs. CCF FWHM (km s^{-1}) using a similar relation as used by Melo et al. (2001); Pace & Pasquini (2004); Hekker & Meléndez (2007), which resulted in the following calibration: $v \sin i = \sqrt{(0.73 \pm 0.02) [\text{FWHM}^2 - v_{\text{macro}}^2] - (5.97 \pm 0.01)^2} \text{ km s}^{-1}$ (estimation performed with the MCMC code emcee¹⁰ Foreman-Mackey et al. 2013). The scatter between the measured $v \sin i$ and the ones estimated from CCF is $\sigma = 0.20 \text{ km s}^{-1}$ (excluding the outlier HIP 103983). The typical uncertainty in the rotational velocities we obtain with our method – line profile fitting with extreme high resolution spectra – is 0.12 km s^{-1} , which implies that the average error of the CCF FWHM $v \sin i$ scaling is 0.16 km s^{-1} , which could be significantly higher if the broadening by v_{macro} is not accounted for.

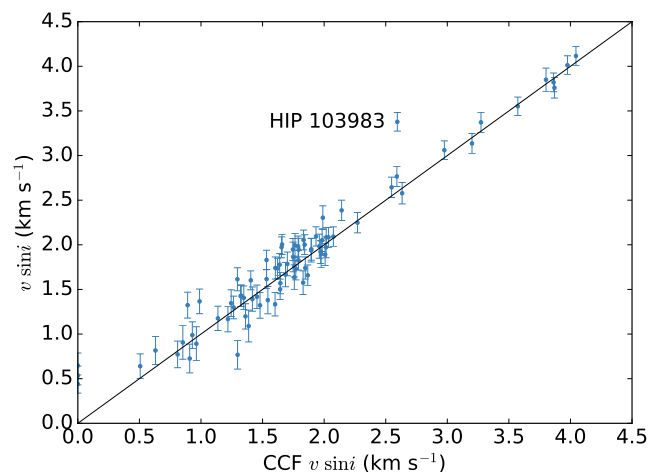


Fig. 4. Comparison between our estimated values of $v \sin i$ (y-axis) and the ones inferred from the cross-correlation function FWHM (x-axis). The spread around the 1:1 relation (black line) is $\sigma = 0.20 \text{ km s}^{-1}$.

4. Binary stars

We identified 16 spectroscopic binaries (SB) in our sample of 82 solar twins by analyzing their radial velocities; some of these stars are reported as binaries by Tokovinin (2014a,b); Mason et al. (2001); Baron et al. (2015). We did not find previous reports of multiplicity for the stars HIP 30037, HIP 62039 and HIP 64673 in the literature. Our analysis of variation in the HARPS radial velocities suggest that the first two are probable SBs, while the latter is a candidate. No binary shows a double-lined spectrum, but HIP 103983 has distortions that could be from contamination by a companion. The star HIP 64150 is a Sirius-like system with a directly observed white dwarf companion (Crepp et al. 2013; Matthews et al. 2014). The sample from Paper I contains another SB, HIP 109110, for which we could not reliably determine the $v \sin i$ due to strong contamination in the spectra, possibly caused by a relatively bright companion. Thus, we did not include this star in our sample.

Of these 16 spectroscopic binaries, at least four of them (HIP 19911, 43297, 67620 and 73241) show unusually high $v \sin i$ (see the left panel of Fig. 5). These stars also present other anomalies, such as their $[Y/Mg]$ abundances (Tucci Maia et al. 2016) and magnetic activity (Ramírez et al. 2014; Freitas et al. 2016). The solar twin blue straggler HIP 10725 (Schirbel et al. 2015), which is not included in our sample, also shows a high $v \sin i$ for its age. We find that five of the binaries have rotational velocities below the expected for Sun-like stars, but this is most likely an effect of projection of the stars' rotational axes. For the remaining binaries, which follow the rotational braking law, it is again difficult to disentangle this behavior from the $\sin i$, and a statistical analysis is precluded by the low numbers involved. Tidal interactions between companions that could potentially enhance rotation depend on binary separation, which is unknown for most of these stars. They should be regular rotators, since they do not show anomalies in chromospheric activity (Freitas et al. 2016) or $[Y/Mg]$ abundances (Tucci Maia et al. 2016).

Based on the information that at least 25% of the spectroscopic binaries in our sample show higher rotational velocities than expected for single stars, we conclude that stellar multiplicity is an important enhancer of rotation in Sun-like stars. Blue stragglers are expected to have a strong enhancement on rotation

⁹ This is the same recipe adopted by the radiative transfer code MOOG.

¹⁰ Available at <http://dan.iel.fm/emcee/current/>

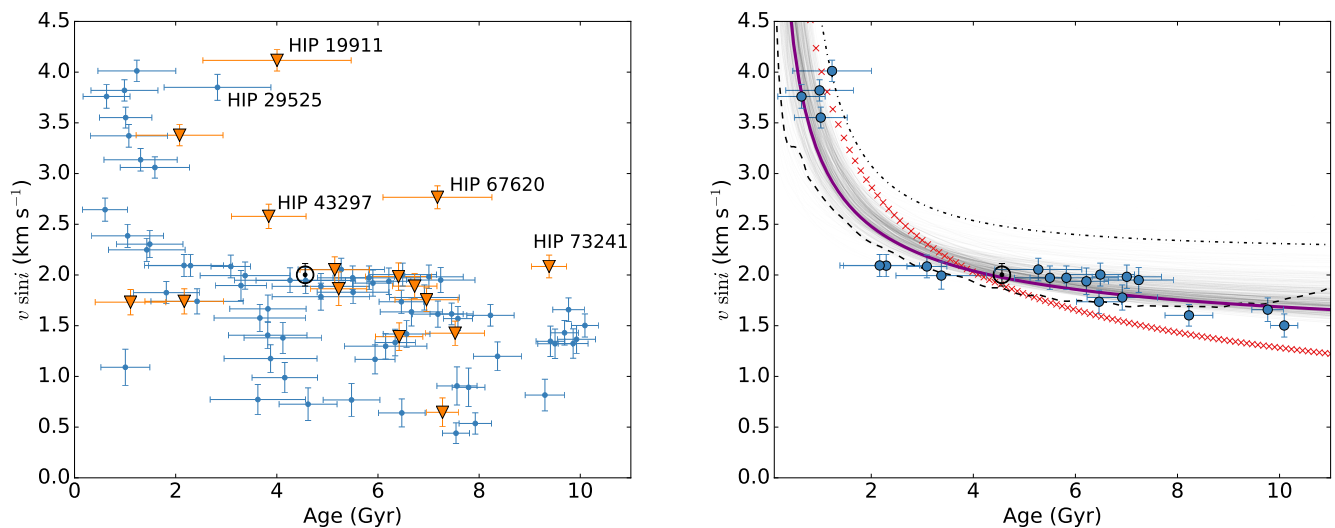


Fig. 5. Projected rotational velocity of solar twins in function of their age. The Sun is represented by the symbol \odot . Left panel: all stars of our sample; the orange triangles are spectroscopic binaries, blue circles are the remaining non-spectroscopic binaries. Right panel: the rotational braking law; the purple continuous curve is our relation inferred from fitting the *selected sample* (blue circles) of solar twins with the form $v \sin i = v_f + m t^{-b}$, where t is the stellar age, and the fit parameters are $v_f = 1.224 \pm 0.447$, $m = 1.932 \pm 0.431$ and $b = 0.622 \pm 0.354$, with v_f and b highly and positively correlated. The light grey region is composed of 300 curves that are created with parameters drawn from a multivariate gaussian distribution defined by the mean values of the fit parameters and their covariance matrix. Skumanich's law (red \times symbols, calibrated for $v_{\text{rot}}^{\odot} = 1.9 \text{ km s}^{-1}$) and the rotational braking curves proposed by do Nascimento et al. (2014, black dashed curve, smoothed) and Pace & Pasquini (2004, black dot-dashed curve) are plotted for comparison.

due to injection of angular momentum from the donor companion.

5. The rotational braking law

In order to correctly constrain the rotational braking, we removed from this analysis all the spectroscopic binaries. The non-SB HIP 29525 displays a $v \sin i$ much higher than expected ($3.85 \pm 0.13 \text{ km s}^{-1}$), but it is likely that this is due to an overestimated isochronal age ($2.83 \pm 1.06 \text{ Gyr}$). Because it is a clear outlier in our results, we decided to not include HIP 29525 in the rotational braking determination. Maldonado et al. (2010) found X-ray and chromospheric ages of 0.55 and 0.17 Gyr, respectively, for HIP 29525. We then divided the remaining 65 stars and the Sun in bins of 2 Gyr, and removed from this sample all the stars which were below the 70th percentile of $v \sin i$ in each bin¹¹. This allowed us to select the stars that had the highest chance of having $\sin i$ above 0.9. In total, 21 solar twins and the Sun compose what we hereafter reference as the *selected sample*. Albeit this sub-sample is smaller, it has the advantage of mostly removing uncertainties on the inclination angle of the stellar rotation axes¹². We stress that the only reason we can select the most probable edge-on rotating stars ($i = \pi/2$) is because we have a large sample of solar twins in the first place.

We then proceeded to fit a general curve to the *selected sample* (see Fig. 5) using the method of orthogonal distance regression (ODR, Boggs & Rogers 1990), which takes into account the uncertainties on both $v \sin i$ and ages. This curve is a power law plus constant of the form $v = v_f + m t^{-b}$ (the same chromospheric activity and $v \sin i$ vs. age relation used by Pace &

¹¹ By doing a simple simulation with angles i drawn from a flat distribution between 0 and $\pi/2$, we verify that 30% of the stars should have $\sin i$ above 0.9.

¹² This procedure can also allow for unusually fast-rotating stars (although rare) with $\sin i$ below 0.9 to leak into our sample.

Pasquini 2004; Guinan & Engle 2009), with v (rotational velocity) and v_f (asymptotic velocity) in km s^{-1} and t (age) in Gyr.

We find that the best fit parameters are $v_f = 1.224 \pm 0.447$, $m = 1.932 \pm 0.431$ and $b = 0.622 \pm 0.354$ (see right panel of Fig. 5). These large uncertainties are likely due to: i) the strong correlation between v_f and b ; and ii) the relatively limited number of datapoints between 1 and 4 Gyr, where the parameter is most effective in changing the values of v . This limitation is also present in past studies (e.g., van Saders et al. 2016; Barnes 2003; Pace & Pasquini 2004; Mamajek & Hillenbrand 2008; García et al. 2014; Amard et al. 2016). On the other hand, our sample is the largest comprising solar twins, and therefore should produce more reliable results. With more datapoints, we could be able to use 1 Gyr bins instead of 2 Gyr in order to select the fastest rotating stars, which would result in a better sub-sample for constraining the rotational evolution for young stars.

The relation we obtain is in contrast with some previous studies on modelling the rotational braking (Barnes 2001, 2003; Lanzafame & Spada 2015) which either found or assumed that the Skumanich's law explains well the rotational braking of Sun-like stars. The conclusions by van Saders et al. (2016) limit the range of validation up to approximately the solar age (4 Gyr) for stars with solar mass. When we enforce the Skumanich's power law index $b = 1/2$, we obtain a worse fit between the ages 2 and 4 Gyr (and, not surprisingly, also after the solar age).

Our data and the rotational braking law that results from them show that the Sun is a normal star regarding its rotational velocity when compared to solar twins. However, they do not agree with a regular Skumanich's law (Barnes 2007, red \times symbols in Fig. 5). We find a better agreement with the model proposed by do Nascimento et al. (2014, black dashed curve in Fig. 5), especially for stars older than 2 Gyr. This model is thoroughly described in Appendix A of do Nascimento et al. (2012). In summary, it uses an updated treatment of the instabilities relevant to the transport of angular momentum according to Zahn (1992)

and Talon & Zahn (1997), with an initial angular momentum for the Sun $J_0 = 1.63 \times 10^{50} \text{ g cm}^2 \text{ s}^{-1}$. Its corresponding rotational braking curve is computed using the output radii of the model, which vary from $\sim 1 R_\odot$ at the current solar age to $1.57 R_\odot$ at the age of 11 Gyr, and it changes significantly if we use a constant radius $R = 1 R_\odot$, resulting in a more Skumanich-like rotational braking.

Our result agrees with the chromospheric activity vs. age behavior for solar twins obtained by Ramírez et al. (2014), in which a steep decay of the R'_{HK} index during the first 4 Gyr was deduced (see Fig. 11 in their paper). The study by Pace & Pasquini (2004) also suggests a steeper power-law index ($b = 1.47$) than Skumanich's ($b_S = 1/2$) in the rotational braking law derived from young open clusters, the Sun and M 67. However, as seen in Fig. 5, their relation significantly overestimates the rotational velocities of stars, especially for those older than 2 Gyr. This is most probably caused by other line broadening processes, mainly the macroturbulence, which were not considered in that study. As we saw in Sect. 3.1, those introduce important effects that are sometimes larger than the rotational broadening. Moreover, a CCF-only analysis tends to produce more spread in the $v \sin i$ than the more detailed analysis we used.

The rotational braking law we obtain produces a similar outcome to that achieved by van Saders et al. (2016) for stars older than the Sun (a weaker rotational braking law after solar age than previously suggested). Our data also requires a different power law index than Skumanich's index for stars younger than the Sun, one that accounts for an earlier decay of rotational velocities up to 2 Gyr.

The main sequence spin-down model by Kawaler (1988) states that, for constant moment of inertia and radius during the main sequence, we would have

$$v_{\text{eq}} \propto t^{-3/(4an)}, \quad (3)$$

where v_{eq} is the rotational velocity at the equator and a and n are parameters that measure the dependence on rotation rate and radius, respectively (see Eqs. 7, 8 and 12 in their paper). If we assume a dipole geometry for the stellar magnetic field ($B_r \propto B_0 r^{-3}$), then $n = 3/7$. Furthermore, assuming that $a = 1$, then Eq. 3 results in $v_{\text{eq}} \propto t^{-7/4} = t^{-1.75}$. Skumanich's law ($v_{\text{eq}} \propto t^{-0.5}$) is recovered for $n = 3/2$, which is close to the case of a purely radial field ($n = 2$, $v_{\text{eq}} \propto t^{-0.38}$). A more extensive exploration of the configuration and evolution of magnetic fields of solar twins is outside the scope of this paper, but our results suggest that the rotational braking we observe on this sample of solar twins stems from a magnetic field with an intermediate geometry between dipole and purely radial.

6. Conclusions

We analyzed the rotational velocities of 82 bright solar twins in the Southern Hemisphere and the Sun using extremely high resolution spectra. Radial velocities revealed that our sample contained 16 spectroscopic binaries, three of which (HIP 30037, 62039, 64673) were not listed as so in the literature. At least five of these stars show an enhancement on their measured $v \sin i$, which is probably caused by interaction with their close-by companions. They also present other anomalies in chemical abundances and chromospheric activities. We did not clearly identify non-spectroscopic binary stars with unusually high rotational velocities for their age.

In order to better constrain the rotational evolution of the solar twins, we selected a subsample of stars with higher chances

of having their rotational axis inclination close to $\pi/2$ (almost edge-on). We opted to use carefully measured isochronal ages for these stars because it is the most reliable method available for this sample. We finally conclude that the Sun seems to be a common rotator, within our uncertainties, when compared to solar twins, therefore it can be used to calibrate stellar models.

Moreover, we have found that Skumanich's law does not describe well the rotation evolution for solar twins observed in our data, a discrepancy that is stronger after the solar age. Therefore, we propose a new rotational braking law that supports the weakened braking after the age of the Sun, and comes with a earlier decay in rotational velocities up to 2 Gyr than the classical Skumanich's law. Interestingly, it also reveals an evolution that is more similar to the magnetic activity evolution observed in Sun-like stars, which sees a steep decay in the first 3 Gyr and flattens near the solar age. Additionally, we suggest that more high-precision spectroscopic observations of solar twins younger and much older than the Sun could help us better constrain the rotational evolution of solar-like stars.

Acknowledgements. LdS thanks CAPES and FAPESP, grants no. 2014/26908-1 and 2016/01684-9 for support. JM thanks for support by FAPESP (2012/24392-2). LS acknowledges support by FAPESP (2014/15706-9). We also would like to thank the anonymous referee for the valuable comments that significantly improved this manuscript.

References

- Amard, L., Palacios, A., Charbonnel, C., Gallet, F., & Bouvier, J. 2016, *A&A*, 587, A105
- Bahcall, J. N., Pinsonneault, M. H., & Wasserburg, G. J. 1995, *Reviews of Modern Physics*, 67, 781
- Baliunas, S. L., Donahue, R. A., Soon, W. H., et al. 1995, *ApJ*, 438, 269
- Barnes, S. A. 2001, *ApJ*, 561, 1095
- Barnes, S. A. 2003, *ApJ*, 586, 464
- Barnes, S. A. 2007, *ApJ*, 669, 1167
- Baron, F., Lafrenière, D., Artigau, É., et al. 2015, *ApJ*, 802, 37
- Baumann, P., Ramírez, I., Meléndez, J., Asplund, M., & Lind, K. 2010, *A&A*, 519, A87
- Bedell, M., Meléndez, J., Bean, J. L., et al. 2015, *A&A*, 581, A34
- Bedell, M., Meléndez, J., Bean, J. L., et al. 2014, *ApJ*, 795, 23
- Biazzo, K., Gratton, R., Desidera, S., et al. 2015, *A&A*, 583, A135
- Boggs, P. T. & Rogers, J. E. 1990, *Contemporary Mathematics*, 112, 183
- Castelli, F. & Kurucz, R. L. 2004, *ArXiv Astrophysics e-prints* [astro-ph/0405087]
- Ceillier, T., García, R. A., Salabert, D., & Mathur, S. 2015, in *European Physical Journal Web of Conferences*, Vol. 101, European Physical Journal Web of Conferences, 06016
- Chaplin, W. J., Basu, S., Huber, D., et al. 2014, *ApJS*, 210, 1
- Charbonneau, P. 1992, in *Astronomical Society of the Pacific Conference Series*, Vol. 26, Cool Stars, Stellar Systems, and the Sun, ed. M. S. Giampapa & J. A. Bookbinder, 416
- Charbonnel, C., Vauclair, S., Maeder, A., Meynet, G., & Schaller, G. 1994, *A&A*, 283, 155
- Crepp, J. R., Johnson, J. A., Howard, A. W., et al. 2013, *ApJ*, 774, 1
- do Nascimento, J.-D., da Costa, J. S., & Castro, M. 2012, *A&A*, 548, L1
- do Nascimento, Jr., J.-D., García, R. A., Mathur, S., et al. 2014, *ApJ*, 790, L23
- do Nascimento, Jr., J.-D., Vidotto, A. A., Petit, P., et al. 2016, *ApJ*, 820, L15
- Doyle, A. P., Davies, G. R., Smalley, B., Chaplin, W. J., & Elsworth, Y. 2014, *MNRAS*, 444, 3592
- Foreman-Mackey, D., Hogg, D. W., Lang, D., & Goodman, J. 2013, *PASP*, 125, 306
- Freitas, F. C., Meléndez, J., Bedell, M., et al. 2016, In preparation
- Gallet, F. & Bouvier, J. 2013, *A&A*, 556, A36
- García, R. A., Ceillier, T., Salabert, D., et al. 2014, *A&A*, 572, A34
- Gray, D. F. 1984, *ApJ*, 281, 719
- Gray, D. F. 2005, *The Observation and Analysis of Stellar Photospheres*
- Guinan, E. F. & Engle, S. G. 2009, in *IAU Symposium*, Vol. 258, The Ages of Stars, ed. E. E. Mamajek, D. R. Soderblom, & R. F. G. Wyse, 395–408
- Gustafsson, B. 1998, *Space Sci. Rev.*, 85, 419
- Hekker, S. & Meléndez, J. 2007, *A&A*, 475, 1003
- Howard, R. & Harvey, J. 1970, *Sol. Phys.*, 12, 23
- Kawaler, S. D. 1988, *ApJ*, 333, 236

- Lanzafame, A. C. & Spada, F. 2015, A&A, 584, A30
- Leão, I. C., Pasquini, L., Ferreira Lopes, C. E., et al. 2015, A&A, 582, A85
- Magic, Z., Collet, R., Asplund, M., et al. 2013, A&A, 557, A26
- Maldonado, J., Martínez-Arnáiz, R. M., Eiroa, C., Montes, D., & Montesinos, B. 2010, A&A, 521, A12
- Mamajek, E. E. & Hillenbrand, L. A. 2008, ApJ, 687, 1264
- Mason, B. D., Hartkopf, W. I., Holdenried, E. R., & Rafferty, T. J. 2001, AJ, 121, 3224
- Matthews, C. T., Crepp, J. R., Skemer, A., et al. 2014, ApJ, 783, L25
- Mayor, M., Pepe, F., Queloz, D., et al. 2003, The Messenger, 114, 20
- Meléndez, J., Bergemann, M., Cohen, J. G., et al. 2012, A&A, 543, A29
- Melo, C. H. F., Pasquini, L., & De Medeiros, J. R. 2001, A&A, 375, 851
- Noyes, R. W., Hartmann, L. W., Baliunas, S. L., Duncan, D. K., & Vaughan, A. H. 1984, ApJ, 279, 763
- Pace, G. & Pasquini, L. 2004, A&A, 426, 1021
- Pinsonneault, M. H., Kawaler, S. D., Sofia, S., & Demarque, P. 1989, ApJ, 338, 424
- Pizzolato, N., Maggio, A., Micela, G., Sciortino, S., & Ventura, P. 2003, A&A, 397, 147
- Ramírez, I., Allende Prieto, C., & Lambert, D. L. 2013, ApJ, 764, 78
- Ramírez, I., Meléndez, J., Bean, J., et al. 2014, A&A, 572, A48
- Ribas, I., Guinan, E. F., Güdel, M., & Audard, M. 2005, ApJ, 622, 680
- Robles, J. A., Lineweaver, C. H., Grether, D., et al. 2008, ApJ, 684, 691
- Saffe, C., Flores, M., & Buccino, A. 2015, A&A, 582, A17
- Schirbel, L., Meléndez, J., Karakas, A. I., et al. 2015, A&A, 584, A116
- Skumanich, A. 1972, ApJ, 171, 565
- Smith, M. A. 1979, PASP, 91, 737
- Snedden, C. A. 1973, PhD thesis, THE UNIVERSITY OF TEXAS AT AUSTIN.
- Soderblom, D. R. 1983, ApJS, 53, 1
- Soderblom, D. R. 1985, AJ, 90, 2103
- Soderblom, D. R., Duncan, D. K., & Johnson, D. R. H. 1991, ApJ, 375, 722
- Soderblom, D. R., Stauffer, J. R., Hudon, J. D., & Jones, B. F. 1993, ApJS, 85, 315
- Sood, A., Kim, E.-j., & Hollerbach, R. 2016, ArXiv e-prints [arXiv:1605.07125]
- Strassmeier, K. G., Weber, M., Granzer, T., & Järvinen, S. 2012, Astronomische Nachrichten, 333, 663
- Talon, S. & Zahn, J.-P. 1997, A&A, 317, 749
- Tokovinin, A. 2014a, AJ, 147, 86
- Tokovinin, A. 2014b, AJ, 147, 87
- Tucci Maia, M., Meléndez, J., Castro, M., et al. 2015, A&A, 576, L10
- Tucci Maia, M., Ramírez, I., Meléndez, J., et al. 2016, A&A, 590, A32
- van Saders, J. L., Ceillier, T., Metcalfe, T. S., et al. 2016, Nature, 529, 181
- Yana Galarza, J., Meléndez, J., Ramírez, I., et al. 2016, A&A, 589, A17
- Yi, S., Demarque, P., Kim, Y.-C., et al. 2001, ApJS, 136, 417
- Zahn, J.-P. 1992, A&A, 265, 115

Table 3. Ages, the measured $v \sin i$ and stellar parameters of the 82 solar twins and the Sun.

Star	Age	σ	$v \sin i$	σ	[Fe/H]	σ	T_{eff}	σ	$\log g$	σ	v_t	σ	v_{macro}
	(Gyr)		(km s ⁻¹)		(dex)		(K)		(cgs)		(km s ⁻¹)		(km s ⁻¹)
HIP 1954	4.87	0.97	1.79	0.13	-0.068	0.006	5717	5	4.46	0.02	0.96	0.02	2.90
HIP 3203 [†]	0.99	0.66	3.82	0.11	-0.087	0.008	5850	10	4.52	0.02	1.16	0.02	3.27
HIP 4909 [†]	1.23	0.77	4.01	0.11	0.028	0.008	5854	10	4.50	0.02	1.12	0.02	3.33
HIP 5301 [†]	6.49	0.67	2.00	0.12	-0.064	0.004	5728	5	4.42	0.02	0.97	0.01	3.01
HIP 6407*	1.49	0.66	2.30	0.13	-0.068	0.007	5764	8	4.52	0.01	0.97	0.02	2.96
HIP 7585	3.29	0.51	1.90	0.15	0.095	0.005	5831	5	4.43	0.01	1.02	0.01	3.37
HIP 8507	3.63	0.94	0.77	0.15	-0.096	0.006	5725	6	4.49	0.02	0.99	0.02	2.88
HIP 9349	1.43	0.76	2.25	0.11	0.009	0.007	5810	8	4.50	0.02	1.07	0.02	3.16
HIP 10175	1.82	0.65	1.83	0.11	-0.007	0.005	5738	7	4.51	0.01	0.96	0.01	2.89
HIP 10303	5.48	0.56	0.77	0.16	0.106	0.004	5725	4	4.40	0.01	0.98	0.01	3.04
HIP 11915	4.16	0.65	0.99	0.15	-0.059	0.004	5760	4	4.46	0.01	0.97	0.01	3.05
HIP 14501	9.93	0.37	1.37	0.14	-0.133	0.005	5728	7	4.29	0.02	1.03	0.01	3.25
HIP 14614 [‡]	5.82	1.02	1.97	0.12	-0.099	0.008	5784	9	4.42	0.03	1.03	0.02	3.21
HIP 15527	7.92	0.32	0.54	0.11	-0.051	0.005	5785	5	4.32	0.01	1.05	0.01	3.40
HIP 18844	7.46	0.43	1.62	0.11	0.016	0.004	5736	5	4.36	0.02	0.99	0.01	3.15
HIP 19911*	4.00	1.47	4.12	0.11	-0.070	0.011	5764	12	4.47	0.04	1.02	0.03	3.05
HIP 22263	1.07	0.76	3.37	0.11	0.030	0.007	5840	8	4.50	0.02	1.08	0.02	3.27
HIP 25670	4.12	0.77	1.38	0.15	0.057	0.005	5771	5	4.44	0.02	1.00	0.01	3.13
HIP 28066	9.86	0.30	1.32	0.15	-0.128	0.004	5733	5	4.29	0.01	1.05	0.01	3.27
HIP 29432	5.51	0.71	1.83	0.11	-0.096	0.005	5758	5	4.44	0.01	1.01	0.01	3.08
HIP 29525	2.83	1.06	3.85	0.13	-0.022	0.007	5737	7	4.49	0.02	1.12	0.02	2.92
HIP 30037*	6.96	0.62	1.76	0.12	-0.011	0.004	5668	5	4.42	0.01	0.94	0.01	2.81
HIP 30158	4.57	0.98	1.95	0.13	0.003	0.006	5702	5	4.46	0.02	0.94	0.02	2.85
HIP 30476	9.69	0.27	1.43	0.12	-0.022	0.004	5710	5	4.26	0.01	1.03	0.01	3.24
HIP 30502 [‡]	7.01	0.68	1.98	0.12	-0.076	0.006	5721	6	4.41	0.02	0.98	0.02	3.01
HIP 33094 [†]	10.09	0.27	1.50	0.12	0.043	0.005	5662	7	4.16	0.02	1.13	0.01	3.26
HIP 34511 [†]	3.37	0.89	1.99	0.13	-0.103	0.006	5819	6	4.47	0.02	1.03	0.02	3.25
HIP 36512	7.19	0.50	1.61	0.13	-0.117	0.004	5737	4	4.41	0.01	0.99	0.01	3.06
HIP 36515 [‡]	0.63	0.46	3.76	0.12	-0.021	0.009	5847	12	4.54	0.02	1.17	0.02	3.23
HIP 38072	1.31	0.72	3.14	0.11	0.058	0.007	5849	8	4.49	0.02	1.14	0.02	3.33
HIP 40133 [‡]	5.50	0.39	1.97	0.12	0.128	0.004	5755	4	4.37	0.01	1.01	0.01	3.20
HIP 41317 [‡]	8.22	0.47	1.60	0.11	-0.068	0.004	5700	5	4.38	0.01	0.96	0.01	2.99
HIP 42333 [‡]	1.01	0.52	3.55	0.10	0.138	0.008	5848	8	4.50	0.02	1.16	0.02	3.30
HIP 43297*	3.84	0.74	2.58	0.12	0.083	0.006	5702	5	4.46	0.01	0.99	0.02	2.85
HIP 44713	7.58	0.29	1.57	0.12	0.088	0.005	5768	6	4.28	0.01	1.06	0.01	3.41
HIP 44935 [†]	6.22	0.43	1.94	0.13	0.058	0.005	5782	5	4.37	0.01	1.04	0.01	3.30
HIP 44997	3.88	0.92	1.18	0.14	-0.023	0.005	5731	5	4.47	0.02	0.95	0.01	2.93
HIP 49756	4.62	0.57	0.73	0.16	0.043	0.004	5795	4	4.42	0.01	1.01	0.01	3.25
HIP 54102*	1.11	0.70	1.73	0.13	-0.014	0.007	5820	9	4.51	0.02	1.02	0.02	3.18
HIP 54287	6.34	0.40	1.33	0.13	0.118	0.004	5727	4	4.36	0.01	1.01	0.01	3.12
HIP 54582*	7.28	0.31	0.65	0.14	-0.080	0.005	5875	7	4.27	0.02	1.17	0.01	3.82
HIP 62039*	6.73	0.44	1.89	0.12	0.088	0.005	5753	6	4.35	0.02	1.05	0.01	3.23
HIP 64150*	6.41	0.66	1.98	0.14	0.030	0.007	5747	6	4.39	0.02	1.00	0.02	3.13
HIP 64673*	5.22	0.55	1.86	0.17	-0.030	0.007	5918	8	4.35	0.02	1.21	0.02	3.84
HIP 64713	4.26	1.10	1.95	0.12	-0.067	0.007	5767	8	4.46	0.02	1.00	0.02	3.08
HIP 65708	9.41	0.28	1.35	0.15	-0.066	0.006	5755	6	4.25	0.02	1.09	0.01	3.42
HIP 67620*	7.18	1.08	2.77	0.11	-0.018	0.009	5670	9	4.41	0.03	1.01	0.03	2.83
HIP 68468	5.90	0.40	1.92	0.13	0.065	0.007	5857	6	4.32	0.02	1.13	0.01	3.66
HIP 69645 [†]	5.27	0.85	2.05	0.11	-0.045	0.006	5743	6	4.44	0.02	0.99	0.02	3.03
HIP 72043*	6.42	0.47	1.39	0.14	-0.034	0.007	5842	8	4.35	0.02	1.12	0.02	3.55
HIP 73241*	9.38	0.35	2.08	0.11	0.082	0.007	5669	8	4.27	0.02	1.01	0.02	3.08
HIP 73815	6.57	0.46	1.42	0.13	0.004	0.005	5788	6	4.37	0.02	1.05	0.01	3.32
HIP 74389	1.01	0.48	1.09	0.19	0.077	0.004	5844	5	4.49	0.01	1.07	0.01	3.31
HIP 74432** [†]	9.77	0.31	1.66	0.12	0.037	0.007	5684	8	4.25	0.02	1.09	0.02	3.17
HIP 76114	6.15	0.82	1.30	0.13	-0.037	0.006	5733	6	4.42	0.02	0.97	0.02	3.03
HIP 77052**	3.67	0.91	1.58	0.13	0.036	0.006	5683	5	4.48	0.02	0.96	0.02	2.75
HIP 77883 [†]	7.24	0.68	1.95	0.12	-0.006	0.006	5690	6	4.40	0.02	0.99	0.02	2.92
HIP 79578*	2.17	0.78	1.74	0.12	0.057	0.005	5820	5	4.47	0.01	1.04	0.01	3.25
HIP 79672 [†]	3.09	0.39	2.08	0.11	0.056	0.003	5814	3	4.45	0.01	1.02	0.01	3.27
HIP 79715	6.47	0.46	0.64	0.14	-0.041	0.005	5803	6	4.38	0.02	1.09	0.01	3.35
HIP 81746*	7.53	0.58	1.43	0.12	-0.086	0.004	5715	5	4.40	0.02	0.99	0.01	3.00
HIP 83276**	7.54	0.27	0.50	0.10	-0.089	0.006	5885	8	4.22	0.02	1.23	0.01	3.95

Continued on next page

Table 3 - Continuation

Star	Age (Gyr)	σ	$v \sin i$ (km s ⁻¹)	σ	[Fe/H] (dex)	σ	T_{eff} (K)	σ	log g (cgs)	σ	v_t (km s ⁻¹)	σ	v_{macro} (km s ⁻¹)
HIP 85042	6.66	0.62	1.64	0.14	0.015	0.004	5694	5	4.41	0.02	1.00	0.01	2.91
HIP 87769*	5.15	0.69	2.05	0.13	0.000	0.006	5807	6	4.40	0.02	1.05	0.01	3.33
HIP 89650	3.82	0.76	1.67	0.14	0.000	0.005	5841	5	4.44	0.02	1.08	0.01	3.39
HIP 95962**	3.82	0.78	1.41	0.13	0.023	0.005	5806	5	4.44	0.02	1.04	0.01	3.26
HIP 96160 [†]	2.17	0.78	2.09	0.11	-0.053	0.007	5781	8	4.50	0.02	0.96	0.02	3.06
HIP 101905	1.59	0.69	3.06	0.11	0.057	0.006	5890	6	4.47	0.02	1.07	0.02	3.52
HIP 102040	2.42	0.91	1.74	0.12	-0.093	0.006	5838	6	4.48	0.02	1.05	0.02	3.30
HIP 102152 [†]	6.92	0.69	1.78	0.12	-0.020	0.005	5718	5	4.40	0.02	0.95	0.01	3.01
HIP 103983*	2.08	0.86	3.38	0.10	-0.048	0.008	5752	10	4.51	0.02	0.96	0.02	2.93
HIP 104045 [†]	2.29	0.83	2.09	0.11	0.045	0.005	5831	6	4.47	0.02	1.00	0.01	3.29
HIP 105184	0.60	0.45	2.64	0.11	-0.002	0.009	5833	11	4.50	0.02	0.99	0.02	3.25
HIP 108158	8.36	0.48	1.20	0.15	0.067	0.008	5687	7	4.34	0.02	0.97	0.02	3.02
HIP 108468	7.56	0.40	0.91	0.19	-0.111	0.006	5829	7	4.33	0.02	1.16	0.01	3.54
HIP 109821	9.30	0.39	0.82	0.17	-0.115	0.005	5746	7	4.31	0.02	1.06	0.01	3.28
HIP 114615	1.05	0.71	2.39	0.11	-0.077	0.008	5816	9	4.52	0.02	1.04	0.02	3.15
HIP 115577	9.50	0.34	1.32	0.15	0.036	0.008	5699	9	4.25	0.03	1.12	0.02	3.22
HIP 116906 [†]	6.46	0.44	1.74	0.12	0.010	0.005	5792	6	4.37	0.02	1.05	0.01	3.33
HIP 117367	5.94	0.40	1.17	0.14	0.044	0.007	5871	8	4.32	0.02	1.15	0.02	3.72
HIP 118115	7.79	0.32	0.89	0.19	-0.017	0.006	5808	7	4.28	0.02	1.12	0.01	3.55
Sun [†]	4.56	...	2.04	0.12	0.000	...	5777	...	4.44	...	1.00	...	3.20

Notes. * Spectroscopic binary star; ** visual binary star; [†] *selected sample* stars; v_t are the microturbulence velocities. v_{macro} are inferred from the scaling Eq. 2.